CRYSTALLOGRAPHY REPORTS, 2025, Vol. 70, No. 1, pp. 107–114

NANOMATERIALS, CERAMICS

SYNTHESIS OF NICKEL NANODISCS AND MODIFICATION OF SHELLS OF POLYELECTROLYTE MICROCAPSULES WITH THEM

© 2025 V. V. Sarukhanova[a,*], I. M. Doludenko[a], D. R. Khayretdinova[a,b], V. V. Volkov[a], A. V. Bakirov[a,c], Y. V. Grigoriev[a], D. N. Khmelenin[a], A. V. Mikheev[a], and T. V. Bukreeva[a]

[a] *National Research Center "Kurchatov Institute", Moscow, Russia*
[b] *National University of Science and Technology "MISIS", Moscow, Russia*
[c] *Enikolopov Institute of Synthetic Polymeric Materials, Russian Academy of Sciences, Moscow, Russia*
**e-mail: saruhanova.vika@yandex.ru*

Received November 06, 2024
Revised November 22, 2024
Accepted November 22, 2024

Abstract. Magnetic nickel nanoparticles, especially of anisotropic shape, are increasingly attracting the attention of researchers in the field of biomedicine. In this work, magnetic nickel nanodiscs have been synthesized to modify the shells of polyelectrolyte capsules in order to further create new agents for theranostics based on such a nanocomposite system. To obtain nickel nanoparticles in the form of nanodiscs, the method of alternating electrodeposition of metals in the pores of a polymer track membrane was used. Nanowires with alternating layers of copper and nickel were synthesized, and nickel nanodiscs were isolated by selective etching of copper. The magnetic properties of the nanodiscs were investigated by vibrational magnetometry of an array of nanowires in a polymer matrix. The selected disks were studied by dynamic light scattering, electron microscopy, and small-angle X-ray scattering. The possibility of including nickel nanodiscs in the shells of polyelectrolyte capsules by adsorption on a polycation layer followed by application of a polyanion is demonstrated.

DOI: 10.31857/S00234761250115e9

INTRODUCTION

Magnetic nanoparticles have become some of the most well-known, widely studied, and promising objects in nanotechnology in terms of practical applications. Recently, increasing attention has been given to the biomedical applications of these nanoparticles [1–3]. In particular, they have already been approved for use as contrast agents for MRI and show high potential as drug delivery systems, magnetic sensors, and agents for tumor hyperthermia.

For biomedical purposes, iron oxide nanoparticles – magnetite and maghemite – are the most extensively studied due to their relatively low toxicity compared to other magnetic nanoparticles [1, 2]. There is also a growing interest in nanoparticles of transition metals such as Fe, Co, and Ni. Among these, nickel (Ni) magnetic nanoparticles hold a special place [4]. Metallic nickel exhibits catalytic properties, and due to its abundance in the Earth's crust, its use as a catalyst is economically advantageous [5]. As a result, numerous methods have been developed for synthesizing Ni nanoparticles, primarily for catalytic applications. These methods include both the "top-down" and "bottom-up" approaches [4]. The latter category includes thermal decomposition in emulsions, the sol-gel method, chemical vapor deposition, and other techniques. Additionally, there is increasing research on the "green" synthesis of Ni magnetic nanoparticles, which involves using microorganisms or plant extracts as reducing agents [6–8]. Most of these methods yield nearly spherical particles. However, for biomedical applications, anisotropic particles, which exhibit unique magnetic and adsorption properties, can be particularly promising.

Highly anisotropic magnetic nanoparticles, or nanowires, can be synthesized using the template-assisted method based on electrochemical deposition of metal into the pores of track-etched membranes [9]. It is possible to create nanowires with alternating layers by using an electrolyte containing ions of two metals and periodically changing the deposition voltage [10, 11]. These structures can be fragmented into smaller segments through selective etching [12]. Notably, Cu/Ni multilayered nanowires were previously synthesized using template-assisted electrochemical deposition, and subsequent etching of Cu layers resulted in cylindrical Ni nanoparticles (nanorods) [13].

The biomedical application of Ni magnetic nanoparticles is limited by their relatively high cytotoxicity and systemic toxicity [4]. Additionally, like all nanoparticles in the iron subgroup, nickel

nanoparticles face challenges related to rapid oxidation. These issues are addressed by modifying the particle surface and creating stable protective coatings. Furthermore, embedding magnetic nanoparticles into a polymer matrix can enhance their stability and lead to the biocompatibility of the resulting nanocomposite structure.

In this study, nickel nanodisks synthesized via the template-assisted method were incorporated for the first time into the shells of polyelectrolyte capsules — structures that show promise as new drug delivery systems. Polyelectrolyte capsules, formed through layer-by-layer adsorption of oppositely charged polymer ions, have been actively studied for over 25 years due to their versatile composition and structural tunability, as well as their sensitivity to environmental conditions [14]. Several studies have demonstrated the modification of polyelectrolyte capsules with iron oxide magnetic nanoparticles for magnetic localization of drug carriers and remote capsule disruption under an external magnetic field or ultrasound [15–17]. Such modifications have been achieved through both nanoparticle adsorption [16, 17] and in situ nanoparticle synthesis on the polymer shell [18]. The authors of this study were the first to modify polyelectrolyte capsule shells with nickel nanorods synthesized via the template-assisted method [13]. However, these nanorods have relatively large sizes (their length falls within the submicron range) and tend to aggregate laterally during adsorption. In this work, Ni nanodisks were synthesized using the template-assisted method, followed by their characterization using magnetometry, dynamic light scattering (**DLS**), electron microscopy, and small-angle X-ray scattering (**SAXS**). The study also demonstrated the successful adsorption of these nanodisks onto the shells of polyelectrolyte capsules.

METHODS AND MATERIALS

Materials. The following reagents were used to prepare the samples: $CuSO_4 \cdot 5H_2O$, $NiSO_4 \cdot 7H_2O$, NaCl, H_3BO_3, H_2SO_4, NaOH, NH_4OH (Acros Organics, USA), $CaCl_2 \cdot 2H_2O$ (Carl Roth, Germany), Na_2CO_3 (Th. Geyer, Germany), polyallylamine hydrochloride (**PAH**), sodium polystyrene sulfonate (**PSS**), and trisodium salt of ethylenediaminetetraacetic acid (**EDTA**) (Sigma-Aldrich, Germany). Semi-industrial track-etched membranes based on polyethylene terephthalate (manufactured by JINR, Dubna) were used as the growth matrix, with a thickness of 12 μm, pore diameter of 100 nm, and pore density of 1.2×10^9 cm^{-2}. Deionized water purified using a Millipore Direct-Q3 UV system was used in all experiments.

Nanoparticle Synthesis. For metal electrodeposition, a thin conductive copper layer was first applied to one side of the growth matrix by thermal vacuum evaporation (VUP-4). This layer was then electrochemically reinforced using a solution of $CuSO_4 \cdot 5H_2O$ (200 g/L) and H_2SO_4 (10 g/L), forming a continuous conductive layer that served as the working electrode. A specially designed electrochemical cell (with a deposition area of 2.5 cm^2) was used in this work, developed at the Special Design Bureau of the FSRC "Crystallography and Photonics" RAS. A P-2X potentiostat-galvanostat (Elins, Russia) was used as the current source, allowing real-time recording of the electrochemical deposition process. To obtain nanowires composed of alternating metal layers, an electrolyte solution containing 196.3 g/L $NiSO_4 \cdot 7H_2O$, 6.3 g/L $CuSO_4 \cdot 5H_2O$ and 31.5 g/L H_3BO_3.

After electrodeposition, the polymer matrix was dissolved in a concentrated NaOH solution (6N) at 60°C for 6 hours. The sacrificial copper layers and the copper substrate were then removed by selective etching in an aqueous ammonium hydroxide solution (150 g/L) with the addition of 1 g/L $CuSO_4$ for 72 hours. This composition was chosen for its ability to dissolve copper while having minimal interaction with nickel. After complete copper dissolution, the functional particles were extracted from the solution using a permanent magnet.

Capsule formation. Colloidal particles of calcium carbonate were used as core templates for creating capsules. They were obtained by mass crystallization using a known technique, mixing solutions of sodium carbonate and calcium chloride with a concentration of 0.33 M [19]. The particle suspension was centrifuged for 2–3 min at 5000 rpm and washed three times with deionized water. The resulting microparticles were dried in a drying cabinet at 70°C.

Polymer microcapsules were fabricated using the layer-by-layer (LbL) adsorption method with the polyelectrolytes PAH (polycation) and PSS (polyanion). Initially, 2 mL of an aqueous PAH solution (2 mg/mL in 0.5 M NaCl) was added to 0.015 g of $CaCO_3$ particles. The suspension was mixed for 15 minutes using a mini-shaker, centrifuged for 3 minutes at 5000 rpm, and washed three times with deionized water. The same procedure was then repeated with a 2 mL PSS solution (2 mg/mL in 0.5 M NaCl). To form multilayer capsules, the PAH/PSS bilayer deposition process was repeated. After applying the required number of layers, a 0.2 M aqueous EDTA solution was added to the suspension, incubated on a shaker for 15 minutes, and centrifuged. The samples were then washed twice with deionized water.

Research methods. Vibrating sample magnetometry (VSM) of nanowire arrays in the matrix was performed using a VM-07 magnetometer (Russia) in two field orientations – parallel to the sample plane ("in-plane") and perpendicular to it ("out-of-plane").

The size distribution and ζ-potential of nanoparticles and capsules in aqueous suspension were measured using a Zetasizer Nano ZS (Malvern, UK) at 25°C.

Transmission electron microscopy (**TEM**) analysis was conducted using a Tecnai Osiris microscope (FEI, USA) with an accelerating voltage of 200 kV, a wide-angle dark-field detector, and an EDX spectrometer Bruker SuperX.

The SAXS intensity measurements were performed at the BioSUR station at the Kurchatov synchrotron radiation source [20]. The radiation source was a bending magnet with an induction of 1.7 T and an energy of 8 keV (1.433 Å), with a resolution of dE/E 10^{-3} and a photon flux of 10^9 on the sample. The monochromator was a triangular Si(111) crystal with focusing in the horizontal direction. The mirror was flat with a rhodium coating. The sample was placed in a quartz capillary with a diameter of 1.5 mm and a wall thickness of 10 μm. The beam size was 500 × 350 μm. The angular range of measurements was in scattering vector modules $0.03 < s < 3$ nm^{-1} ($s = (4\pi\sin\theta)/\lambda$, 2θ is the scattering angle). The scattering intensity was recorded by a two-dimensional Pilatus-3 1M detector located at a distance of 2.5 m from the sample. Calibration was performed using a silver behenate diffraction standard. Primary processing of two-dimensional diffraction scattering patterns was performed using the Fit2D program [21]. Solvent measurements were performed under similar conditions, the scattering intensity from which was subtracted from the scattering data by the samples. Primary processing of the obtained experimental SAXS data was performed using the PRIMUS program, and calculation of volume distributions by the sizes of density inhomogeneities was performed using the MIXTURE program, integrated into the ATSAS data analysis package [22].

Volume distributions by particle radii in the spherical approximation from the shape were calculated using the formula [23]:

$$I_k(s) = \int_0^\infty N_k(R)[\nu_k(R)\Delta\rho_k(R)]^2 i_{0k}(s,R)T_k(s)dR,$$

where $\Delta\rho_k(R)$, $\nu_k(R)$ and $i_{0k}(s,R)$ denote the contrast, volume and normalized scattering intensity of a particle of radius R. $N_k(R)$ is the analytical function of the particle size distribution, for which the Schulz–Zimma distribution was used [23]. Since this distribution has one maximum, and the real one can be multimodal, a superposition of several distributions is used, the parameters and relative contributions of which are sought using the nonlinear least squares method [23]. The index k in the formula denotes the number of the partial distribution, $k = 1, ..., K$. In this work, $K = 3$ was used, which turned out to be sufficient to describe the experimental data.

DISCUSSION OF RESULTS

First, using the template synthesis method, nanowires with alternating layers of nickel and copper were obtained. Polymer track-etched membranes were used as templates, with a conductive copper layer deposited on one side via vacuum thermal evaporation, followed by electrochemical thickening. The nanowires were formed by pulsed electrodeposition. The metal layers were deposited step by step by varying the potential. An electrolyte composition previously developed and tested for creating layered structures [13] was used. As a result, at a deposition potential of 1.8 V, magnetic functional nickel layers were formed, while at 0.6 V, sacrificial copper layers were deposited. The deposition potential was switched upon reaching a specific charge passing through the electrochemical cell, allowing for more precise control over the thickness of the deposited layers. In this study, the charge required for copper deposition was 270.7 mC, while for functional layers, it was 86 mC. This charge ratio ensured the formation of copper and nickel layers with approximate thicknesses of 100 nm and 50 nm, respectively. To increase the number of functional particles per unit template area, layered nanowires with 20 deposition cycles of both layers were synthesized.

Since the copper layer thickness is nearly twice that of the nickel layer and equals the nanowire diameter, magnetic dipole interactions between nickel layers and between nanowires are negligible [24]. Therefore, the obtained coercivity (H_c) and remanent magnetization (M/M_s) values for the nanowire array can be considered close to those of Ni nanodisks.

Hysteresis loops for the Ni/Cu layered nanowires were obtained (Fig. 1). The sample exhibits some degree of anisotropy, which may be explained by both the geometry of the structures and their arrangement within the membrane volume. In the normal direction to the sample, H_c (224 Oe) and M/M_s (0.53) values are higher than in the sample plane (167 Oe and 0.3, respectively). These data suggest the formation of an easy magnetization axis oriented along the nanowire axis, i.e., parallel to the normal of nanodisks. Based on the particle geometry, an easy magnetization plane is expected due to their aspect ratio. However, their crystalline structure and the influence of crystalline and magnetodipolar anisotropies may lead to the emergence of an easy axis perpendicular to the nanodisk plane. Assuming that dipole interactions between nickel layers are weak, one can conclude that a dispersion of nanodisks should be magnetized similarly to nanowires along their normal direction. In this direction, M/M_s is approximately 0.5, indicating a random distribution of easy magnetization axes among the particles [25]. This observation is supported by the loose orientation of nickel layers within the membrane volume relative to its plane [10, 11].

After alternating nickel and copper electrodeposition, the polymer template was removed by dissolving it in concentrated sodium hydroxide. In the next step, the

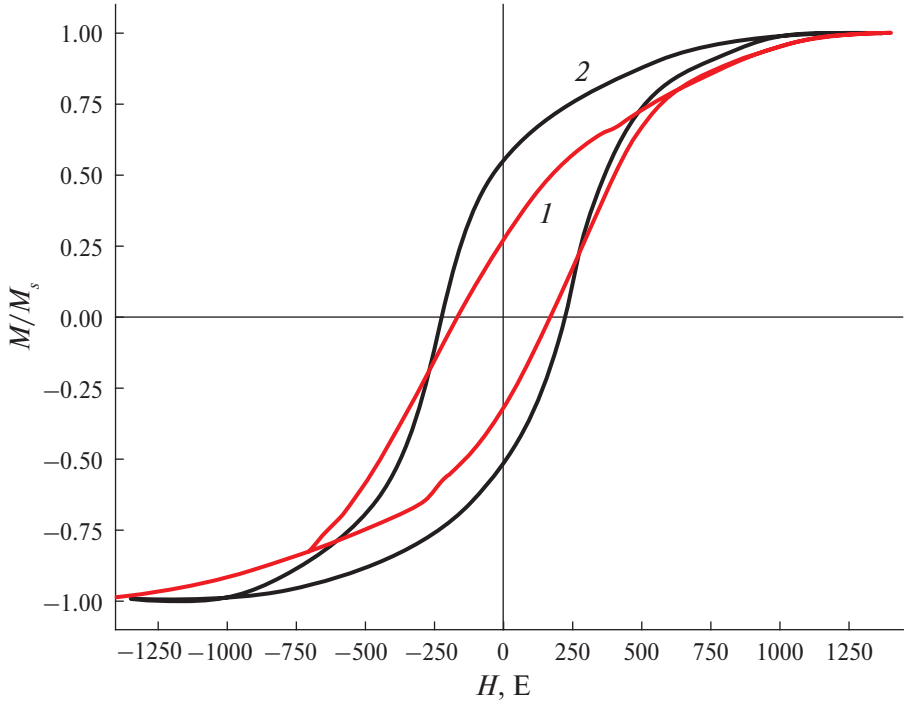

Fig. 1. Hysteresis loops for nanowire samples with a given nickel layer thickness of 50 nm for two field directions: in the plane of the sample (1) and parallel to its normal (2).

multilayer structure was separated into individual layers by dissolving the sacrificial copper layers and the copper substrate.

The obtained nanoparticles were initially characterized using DLS (Fig. 2). The average particle size was 744 ± 73 nm, with a small additional peak at 4.3 μm. These results may be due to either incomplete dissolution of the sacrificial layers or strong aggregation of synthesized nickel nanoparticles in aqueous suspension. The colloidal instability of the suspension, i.e., particle aggregation in water, is confirmed by the low absolute value of the ζ-potential, which was −3.3 ± 0.5 mV.

Electron microscopy methods were used for a more accurate characterization of the obtained particles. Fig. 3 shows examples of the obtained images. It can be concluded that during chemical etching the copper layers were removed and the nickel nanoparticles were separated (Fig. 3a), but their aggregation in the form of formed "stacks" is observed (Fig. 3b). Such aggregation of nanoparticles can be explained by their magnetic nature and the geometry of nanodisks, in which the adhesion of precisely the flat sides is energetically favorable. It is evident from the images that the diameter of the Ni disks approximately corresponds to the diameter of the matrix pores (100 nm), but the thickness of the particles is less than expected based on the deposition mode – not 50, but 35–40 nm. The revealed difference can be associated with the depletion of the electrolyte near the working zone during the deposition of nanowires. However, such a feature should be observed only in the final deposition cycles. Due to the pulsed mode of nanoparticle deposition, as well as their subsequent processing by chemical methods, there is a spread of their geometric parameters, and the anisotropy of sizes does not allow for the accurate processing of a large number of particle images obtained by electron microscopy methods. In this regard, the SAXS method was used to study the particles.

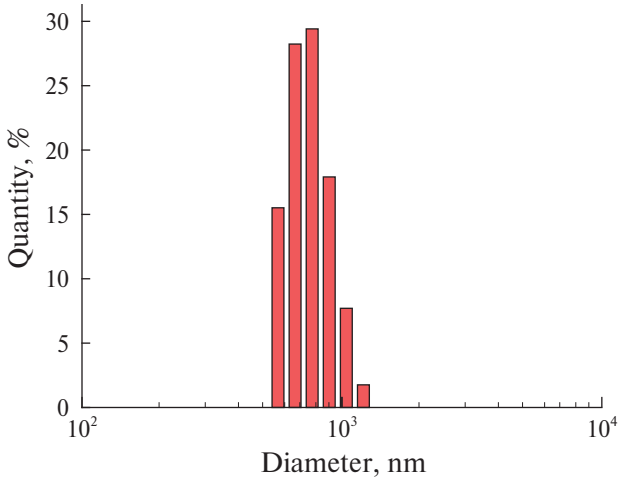

Fig. 2. Distribution of synthesized particles by size according to DLS data.

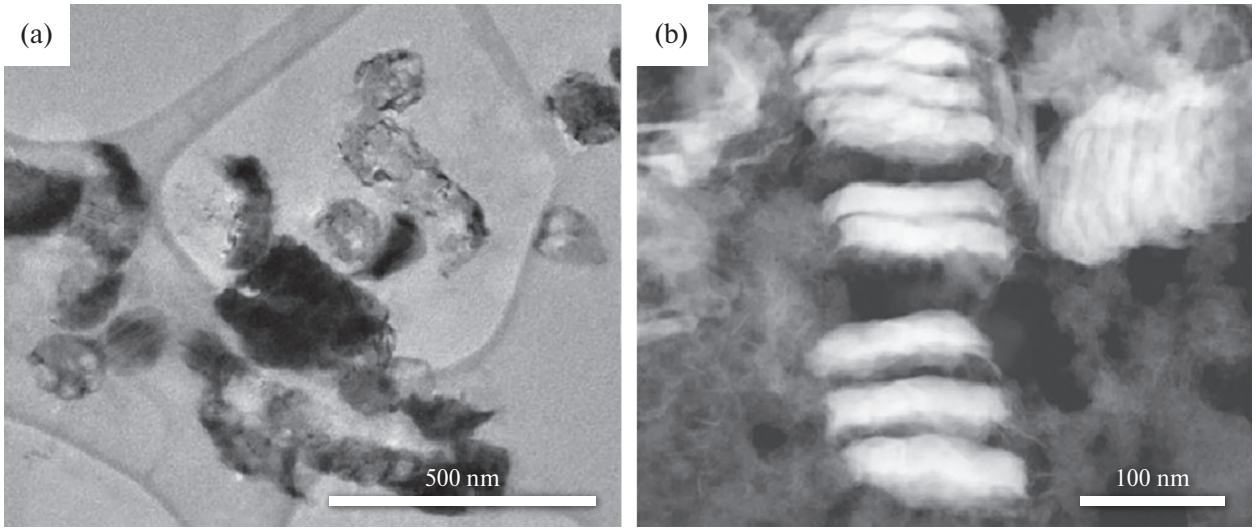

Fig. 3. TEM image of nickel nanoparticles (a) and their image obtained using a ring dark-field detector (b).

The SAXS results are shown in Fig. 4. Note that the particle size distribution is given without taking into account their orientation. Fig. 4a shows the volume distributions by particle radii (i.e. the contribution of particles with a given radius is multiplied by their volume). In general, the size spread is in the range of 5–120 nm with a wide polydisperse background; a maximum of the distribution is visible with an average particle radius of 80–81 nm and a half-width (rms) of 7.9–9.8 nm. With such a small half-width, the Schulz distribution used in the model practically coincides with the Gaussian one. Taking into account the volume of scattering inhomogeneities with sizes less than 5 nm, whose contribution is not shown in the figure, the volume fraction of this narrowly dispersed fraction varies from 0.01 for a concentration of 0.05 μg/ml to 0.06 with an increase in concentration to 0.2 μg/ml. In contrast to this component, the distribution of particles with an average radius of 40–43 nm is wider (rms ~ 30 nm at volume fractions from 0.05 to 0.6). Such a large spread of volume fractions is due to the fact that as the concentration of the system increases, the contribution of small-sized inhomogeneities with radii less than 5 nm decreases from 0.94 to 0.34. Taking into account the particle misorientation, these values correlate with the

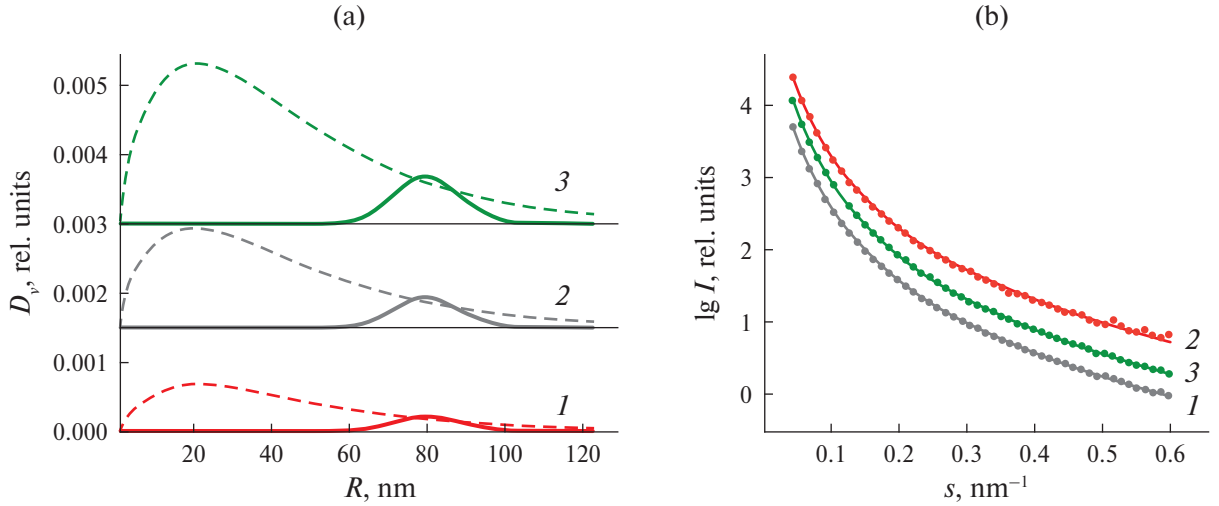

Fig. 4. Volume distributions of particles by the radii of inhomogeneities in the spherical approximation of their shape according to SAXS data (a), particle concentration in suspension: 0.05 (*1*), 0.1 (*2*), 0.2 (*3*) μg/ml. Solid lines correspond to the distribution of the component with a larger size, dashed lines – with a smaller size. Comparison of experimental data with model intensities calculated for the distributions in the figure (a) taking into account the not shown distributions of fractions of small inhomogeneities (b). The intensity curves are shifted vertically for better visualization.

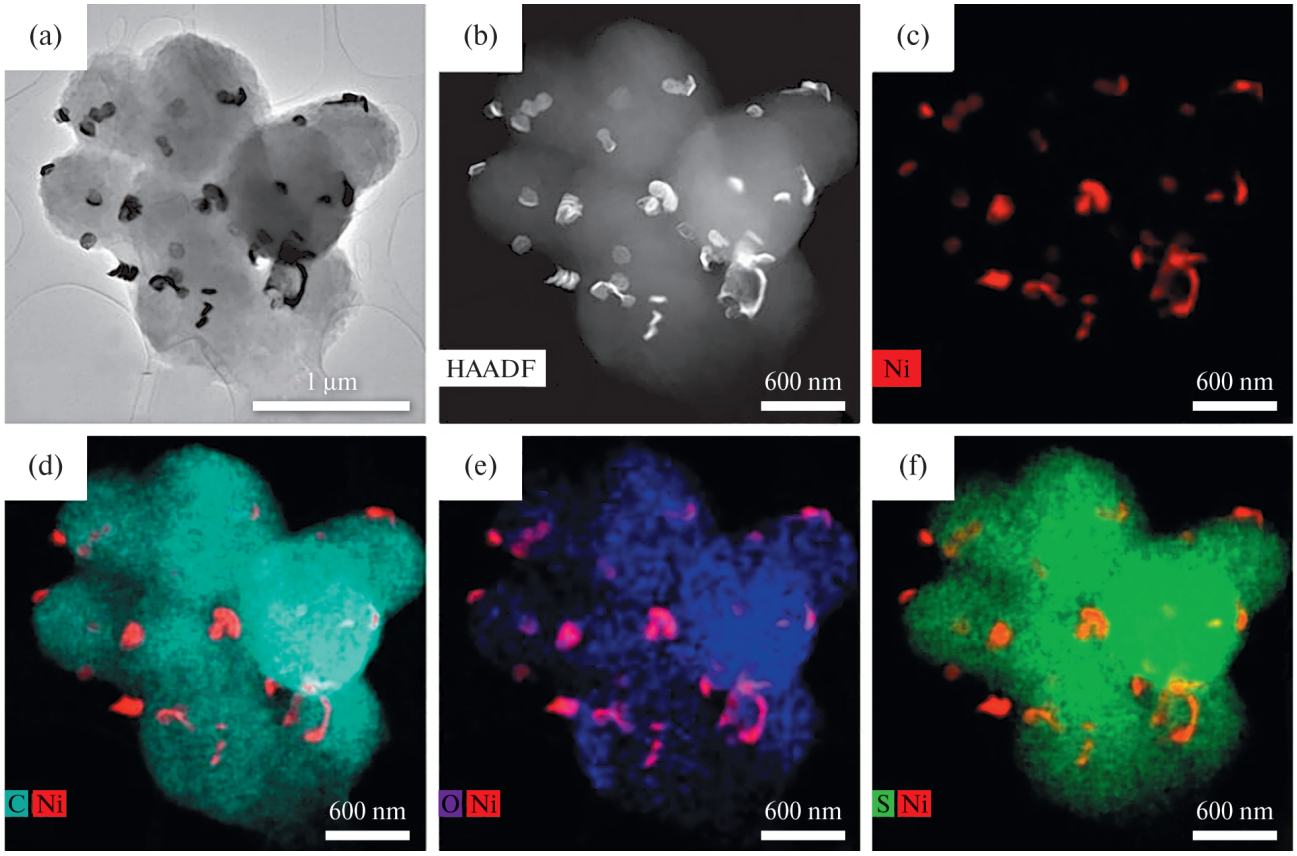

Fig. 5. TEM image of microcapsules modified with nanodisks (a) and their image obtained using a ring dark-field detector (b), as well as distribution maps of nickel (c), carbon (d), oxygen (e), and sulfur (f).

sizes specified at the growth stage. The distribution intensity correlates with the concentration of particles in the solution. The distribution was calculated in the approximation of spherical particles, i.e. the found radii correspond to the radii of equivalent spheres, the volume of which corresponds to the volume of disk particles and is less than the diameters of the disks by no more than 30–40 % (Fig. 3). The model scattering intensities correspond to the size distribution curves of nanodisks (Fig. 4b). The search for the proportions of disk structures in the case of polydispersity of radii and thicknesses according to SAXS data is a mathematically ambiguous problem.

The synthesized nickel nanodisks were incorporated into the shell of polyelectrolyte capsules via electrostatic adsorption. Since the nanodisks have a weakly negative surface charge, they were adsorbed onto a positively charged PAH polyelectrolyte layer. For this, $CaCO_3$-core capsules with a PAH/PSS/PAH shell were centrifuged, and an aqueous suspension of nanodisks at a concentration of 0.2 μg/mL (2 mL suspension per ~10^8 capsules) was added. The system was stirred on a mini-shaker for 15 min, then washed twice with water. After nanodisk adsorption, the ζ-potential of the "core–shell" microparticles changed from +14.1 ± 1.3 to +10.4 ± 0.5 mV. Subsequently, a polyanion (PSS) layer was applied to the microparticle surface, followed by another PAH layer. The adsorption of nickel nanodisks was repeated, covering the particles with an additional PSS layer. As a result, the final shell composition was PAH/PSS/PAH/Ni/PSS/PAH/Ni/PSS. After shell formation, the $CaCO_3$ core was removed using EDTA, as described in the experimental section. The ζ-potential of the final capsules was −21.3 ± 1.1 mV, indicating electrostatic stabilization due to the outer polyanion layer.

The synthesized hollow microcapsules containing nanodisks in the polymer shell were analyzed by TEM and elemental analysis. The obtained images (Fig. 5) confirm the incorporation of nickel nanodisks into the PAH/PSS capsule shell. The distribution of nanoparticles on the capsule surface is fairly uniform, though some aggregates are present.

CONCLUSION

Using the matrix synthesis method based on the electrochemical filling of track-etched membrane pores with metal, nanowires with alternating layers of copper and nickel were fabricated by employing an electrolyte containing ions of both metals and periodically varying

the growth voltage. Process parameters were selected so that, after the removal of "sacrificial" copper layers via chemical etching, nickel nanoparticles in the form of nanodisks were obtained. These anisotropically shaped magnetic nanoparticles were proposed for modifying the shells of polyelectrolyte capsules to enable potential localization of the nanocomposite system within the body and controlled shell disruption under an external magnetic field.

Using magnetometry of the nanowire array within the matrix, the coercive force, saturation field, and easy magnetization axis of the nickel layers – perpendicular to the nanodisk plane – were determined. The coercive force in both directions relative to the nanodisk axis exceeds 100 Oe, indicating the possibility of using fields safe for humans without remagnetizing the nanoparticles.

Electron microscopy methods visualized the chemical separation of the obtained nanodisks, although their aggregation in an aqueous medium was shown. The SAXS and electron microscopy data confirm the formation of nanodisks with sizes corresponding to those specified at the growth stage (100 × 50 nm). Nickel nanodisks were successfully included in the composition of polyelectrolyte capsule shells by their adsorption on a polycation layer. Subsequent application of a polyanion allows electrostatic stabilization of the resulting nanocomposite system.

The set of data obtained in the work demonstrates successful controlled synthesis of nickel nanodisks, formation of nanocomposite capsules with anisotropic magnetic nanoparticles in the shell composition and allows predicting the behavior of magnetic nanodisks, as well as the entire system as a whole in external magnetic fields for local opening of polyelectrolyte microcapsules.

FUNDING

The work was carried out within the framework of the state assignment of the National Research Center "Kurchatov Institute" using the equipment of the Collective Use Center "Structural Diagnostics of Materials" of the Kurchatov Complex of Crystallography and Photonics, as well as the RC of the National Research Center "Kurchatov Institute" (Center for Optical Microscopy and Spectroscopy).

CONFLICT OF INTERESTS

The authors have no conflicts of interest.

REFERENCES

1. *Rezaei B., Yari P., Sanders S.M. et al.* // Small. 2024. V. 20. P. 2304848. https://doi.org/10.1002/smll.202304848
2. *Ullah Khan A., Chen L., Ge G.* // Inorg. Chem. Commun. 2021. V. 134. P. 108995. https://doi.org/10.1016/j.inoche.2021.108995
3. *Materón E.M., Miyazaki C.M., Carr O. et al.* // Appl. Surf. Sci. Adv. 2021. V. 6. P. 100163. https://doi.org/10.1016/j.apsadv.2021.100163
4. *Nuru-Deen Jaji, Hooi Ling Lee, Mohd Hazwan Hussin et al.* // Nanotechnol. Rev. 2020. V. 9. P. 1456. https://doi.org/10.1515/ntrev-2020-0109
5. *Bian Z., Das S., Wai M.H. et al.* // ChemPhysChem. 2017. V. 18. No. 22. P. 3117. https://doi.org/10.1002/cphc.201700529
6. *Gahlawat G., Choudhury A.R.* // RSC Adv. 2019. V. 9. No. 23. P. 12944. https://doi.org/10.1039/c8ra10483b
7. *Sudhasree S., Shakila Banu A., Brindha P., Kurian G.A.* // Toxicol. Env. Chem. 2014. V. 96 (5). P. 743. https://doi.org/10.1080/02772248.2014.923148
8. *Makarov V., Love A., Sinitsyna O. et al.* // Acta Nat. 2014. V. 6. No. 1. P. 20. https://doi.org/10.32607/20758251-2014-6-1-35-44
9. Magnetic Nano- and Microwires: Design, Synthesis, Properties and Applications / Ed. Vazquez M. Elsevier, 2015. P. 962. https://doi.org/10.1016/b978-0-08-102832-2.09989-8
10. *Zhigalina O.M., Doludenko I.M., Khmelenin D.N., Zagorskiy D.L., Bedin S.A. and Ivanov I.M.*// Crystallography Reports. 2018. V. 63, P. 480. https://doi.org/10.1134/S1063774518030379
11. *Zagorskii D.L., Doludenko I. M., Cherkasov D.A., Zhigalina O.M. et al.* // Physics of the Solid State. 2019. V. 61. P. 1634. https://doi.org/10.1134/S1063783419090282
12. *Yao H., Xie L., Cheng Y. et al.* // Mater. Des. 2017. V. 123. No. 5. P. 165. https://doi.org/10.1016/j.matdes.2017.03.041
13. *Doludenko I.M., Mikheev A.E., Burmistrov I.A., Trushina D.B., Borodina T.N., Bukreeva T.V. and Zagorskii D.V.* // Technical Physics. 2020. V. 65. P. 1377. https://doi.org/10.1134/S1063784220090121
14. *Kruk T., Chojnacka-Górka K., Kolasińska-Sojka M., Zapotoczny S.* // Adv. Colloid Interface Sci. 2022. V. 310. P. 102773. https://doi.org/10.1016/j.cis.2022.102773
15. *Timin A.S., Gao H., Voronin D.V. et al.* // Adv. Mater. Interfaces. 2017. V. 4. No. 1. P. 1600338.
16. *Gorin D.A., Portnov S.A., Inozemtseva O.A. et al.* // Phys. Chem. Chem. Phys. 2008. V. 10. P. 6899. https://doi.org/10.1039/b809696a
17. *Burmistrov I.A., Veselov M.M., Mikheev A.V. et al.* // Pharmaceutics. 2022. V. 14. P. 65. https://doi.org/10.3390/pharmaceutics14010065
18. *Lyubutin I.S., Starchikov S.S., Bukreeva T.V. et al.* // Mater. Sci. Eng. C. 2014. V. 45. P. 225. https://doi.org/10.1016/j.msec.2014.09.017

19. *Sukhorukov G.B., Volodkin D.V., Gunther A.M. et al.* // J. Mater. Chem. 2004. V. 14. P. 2073. https://doi.org/10.1039/B402617A
20. *Peters G.S., Zakharchenko O.A., Konarev P.V. et al.* // Nucl. Instrum. Methods Phys. Res. A. 2019. V. 945. P. 162616. https://doi.org/10.1016/ 162616
21. *Hammersley A.P.* // J. Appl. Cryst. 2016. V. 49. P. 646. https://doi.org/10.1107/S1600576716000455
22. *Manalastas-Cantos K., Konarev P.V., Hajizadeh N.R. et al.* // J. Appl. Cryst. 2021. V. 54. P. 343. https://doi.org/10.1107/S1600576720013412
23. *Svergun D.I., Konarev P.V., Volkov V.V. et al.* // J. Chem. Phys. 2000. V. 113. P. 1651. https://doi.org/10.1063/1.481954
24. *Bizyaev D. A., Khairetdinova D. R., Zagorskii D. L., Doludenko I. M., Panina L. V., Bukharaev A. A., and Rizvanova A.* // Physics of Metals and Metallography. 2023. V. 124(8). P. 787. https://doi.org/10.1134/s0031918x23601282
25. *Anikin A.A., Shumskaya E.E., Bedin S.A. et al.* // Bull. Russ. Acad. Sci.: Phys. 2024. V. 88. No. 4. P. 1010. https://doi.org/10.1134/S1062873824706998